applied sciences

MDPI

Article

High-Sensitivity Detection of Carbon Fiber-Reinforced Polymer Delamination Using a Novel Eddy Current Probe

Yingni Zhou [1,2], Bo Ye [1,2,*], Honggui Cao [1,2], Yangkun Zou [2,3], Zhizhen Zhu [4] and Hongbin Xing [1,2]

[1] Faculty of Information Engineering and Automation, Kunming University of Science and Technology, Kunming 650500, China; zyingn_9@163.com (Y.Z.); chgchg2333@163.com (H.C.); xinghongbin@stu.kust.edu.cn (H.X.)
[2] Yunnan Key Laboratory of Intelligent Control and Application, Kunming University of Science and Technology, Kunming 650500, China; zouyangkun@stu.kust.edu.cn
[3] Faculty of Civil Aviation and Aeronautics, Kunming University of Science and Technology, Kunming 650500, China
[4] The First Military Representative Office of the Chongqing Military Representative Bureau of the Army Equipment Department in Kunming, Kunming 650032, China; zhizhen99666@126.com
* Correspondence: yeripple@hotmail.com

Abstract: The demand for non-destructive testing of carbon fiber-reinforced polymer (CFRP) is becoming increasingly pressing to ensure its safety and reliability across different fields of use. However, the complex structural characteristics and anisotropic bulk conductivity of CFRP make achieving high sensitivity in detecting internal defects such as delamination extremely challenging. To address this issue, a novel triple rectangular coil probe with high sensitivity developed for detecting delamination in CFRP is presented in this paper. A finite element model using COMSOL Multiphysics was developed for CFRP delamination eddy current testing with the designed probe. Based on this model, the probe parameters were determined through orthogonal experiments. By analyzing the eddy current distribution in CFRP samples, the scanning mode was defined. Following this, the detection voltage was evaluated for various delamination parameters, and the sensitivity of different probes was compared. Results indicate that, under the same excitation coil parameters, for a 5 mm delamination lateral dimension change, the single pancake and single rectangular coil probes exhibit sensitivities of 88.24% and 72.55%, respectively, compared with the designed probe. For a 0.5 mm delamination thickness change, their sensitivities are 49.04% and 56.69% of those of the designed probe. The designed probe meets the demand for high-sensitivity detection.

Keywords: non-destructive testing; eddy current testing; carbon fiber-reinforced polymer; delamination; high-sensitivity detection

check for updates

Citation: Zhou, Y.; Ye, B.; Cao, H.; Zou, Y.; Zhu, Z.; Xing, H. High-Sensitivity Detection of Carbon Fiber-Reinforced Polymer Delamination Using a Novel Eddy Current Probe. *Appl. Sci.* **2024**, *14*, 3765. https://doi.org/10.3390/app14093765

Academic Editors: Dwayne McDaniel and Cesar Levy

Received: 24 March 2024
Revised: 23 April 2024
Accepted: 25 April 2024
Published: 28 April 2024

1. Introduction

Carbon fiber-reinforced polymer (CFRP) has found widespread applications in aerospace, defense, transportation, and other fields due to its exceptional specific strength, specific stiffness, and corrosion resistance, making it an ideal lightweight structural material [1]. However, during its manufacturing and usage, various types of damages are inevitable, with delamination being one of the major forms [2]. Delamination presents as local separation, insufficient bonding, and cracking between layers. The presence of delamination compromises the integrity of CFRP, impacting its outstanding performance. Moreover, delamination can propagate during service, leading to premature failure of laminates and even causing production accidents [3]. Therefore, delamination is one of the most significant and impactful defects, making non-destructive testing for it crucially important.

The current five major non-destructive testing methods are ultrasonic testing, radiographic testing, magnetic particle testing, penetrant testing, and eddy current testing. They are widely used in various fields due to their respective unique advantages. However,

magnetic particle testing and penetrant testing are inherently difficult to implement in CFRP non-destructive testing due to their characteristics. Magnetic particle testing is a non-destructive testing method that utilizes magnetic changes to detect surface and near-surface defects in ferromagnetic materials. It has advantages such as displaying defects intuitively, high sensitivity, and fast detection speed [4]. However, it has certain limitations since it is only applicable for inspecting ferromagnetic materials (such as steel). Penetrant testing is primarily used to detect surface-opening defects in non-porous metallic and non-metallic components, making it suitable for non-destructive testing of materials such as ceramics and plastics [5]. However, this method is only applicable for detecting defects indicated on the material's surface, and it cannot achieve non-destructive testing for deep-seated or internal defects. Ultrasonic testing, radiographic testing, and eddy current testing are commonly used for non-destructive testing of CFRP [6]. Ultrasonic testing takes advantage of the low density and high elastic modulus of CFRP, allowing ultrasonic waves to penetrate and propagate inside, thereby detecting defects such as delamination and cracks in CFRP [7–9]. However, ultrasonic testing requires a certain level of surface cleanliness on the sample being tested, and the use of a coupling agent is essential during testing. This means that subsequent drying processes for the CFRP sample may have an impact on the testing results. X-rays have strong penetration capabilities and can penetrate CFRP samples. When defects are present in the CFRP, the X-rays are reflected, absorbed, or scattered by the internal defects [10]. However, the expensive equipment and the need for specialized operators limit the widespread application of this technology in CFRP non-destructive testing. Compared with the aforementioned methods, eddy current testing has the advantages of low cost, high efficiency, and no need for a coupling agent, etc. CFRP exhibits orthotropic conductivity, making eddy current testing suitable for detecting delamination. Currently, many scholars have conducted in-depth research on eddy current testing for delamination in CFRP. Mook et al. [11] designed high-frequency eddy-current sensors that can be used to detect delamination. By observing the polar plot of voltage amplitude when the probe rotates to scan CFRP, significant changes in voltage amplitude can be observed at the location of the delamination. Schulze et al. [12] utilized 32 pancake coils to simultaneously detect delamination and conducted imaging studies based on the varying eddy current density at the delamination sites. Koyama et al. [13] utilized a CP probe with a rectangular exciting coil to detect multidirectional artificial delamination in CFRP, and this probe had a high signal-to-noise ratio. Zeng et al. [14–16] conducted theoretical and numerical simulations on eddy current testing of CFRP, confirming that vertically oriented rectangular coil probes are more suitable for detecting delamination than pancake coil probes. They also established a coplanar dual rectangular coil finite element model for detecting delamination, which can be used for delamination detection. Qiu et al. [17] constructed a high-sensitivity eddy current testing system. They utilized this system along with a TR probe to achieve detection and imaging of 200 um delamination in CFRP at a frequency of 2 MHz. Mizukami et al. [18] successfully detected 10 mm $\times$ 10 mm delamination by optimizing the distance between the excitation coil and the detection coil. Machado et al. [19] designed a high-speed eddy current probe that successfully detected delamination in CFRP plates at a frequency of 1 MHz and a speed of 4 m/s, meeting the requirements for high-quality detection. Xu et al. [20] utilized a T-R probe to study the physical mechanism of delamination eddy current testing and conducted detection on delamination in CFRP with different ply orientations. The probes used in the above-mentioned literature were able to detect delamination in CFRP. However, due to the multi-phase heterogeneity and discontinuity in the geometric structure of CFRP, as well as the fact that delamination is an internal defect with relatively small eddy current disturbances, the detection results are susceptible to noise interference, and the probes currently used often have low detection sensitivity, which is not conducive to subsequent quantitative assessment of delamination. Therefore, designing a probe with higher detection sensitivity for delamination in CFRP has become an urgent issue that needs to be addressed.

Pancake coil and rectangular coil are widely used in CFRP eddy current testing, with each type of coil having its advantages. Pancake coils can generate a uniformly distributed magnetic field, which aids in covering the entire testing area. A rectangular coil is directional and can produce a concentrated magnetic field, making defect localization easier. Additionally, rectangular coil probes can induce larger vertical eddy currents, which are more susceptible to disturbances caused by delamination. Therefore, this study designed a novel triple rectangular coil probe based on a rectangular coil. The excitation coils of this probe are dual rectangular coils, while the detection coil is a single rectangular coil. Using dual rectangular excitation coils can induce larger vertical eddy currents in the CFRP sample, thereby increasing the detection voltage. The spatially perpendicular arrangement of the excitation coils and detection coil reduces interference signals during detection and allows the detection coil to maximize the acquisition of defect information. Using COMSOL Multiphysics, a finite element simulation model was developed for CFRP delamination eddy current testing using the probe. Based on this model, an orthogonal experiment was carried out to determine the parameters of the probe, and the scanning modes of the probe were determined by studying the eddy current distribution in the CFRP sample. Subsequently, the influence of delamination of different dimensions on the detection coil voltage signal was studied. Finite element simulation models were established to simulate and calculate the detection voltage values of the novel triple rectangular coil probe, single pancake probe, and single rectangular probe for detecting different sizes of delamination. Based on this, the detection sensitivity of each probe was compared with verify the effectiveness of the designed probe.

2. Principles of Eddy Current Testing and Probe Design

2.1. Principles of Eddy Current Testing

Eddy current testing is based on the electromagnetic induction between the probe and the conductive material being tested [21]. The equivalent circuit diagram of the probe is shown in Figure 1, where the eddy current testing signal comes from the variation in induced voltage in the secondary coil. When an AC current I_1 is passed through the excitation coil, under electromagnetic induction, an induced current I_2 is generated in the detection coil. Conversely, I_2 also affects the relationship between current and voltage in the excitation coil. Moreover, there is mutual inductance M_{12} (M_{21}) between the two coils.

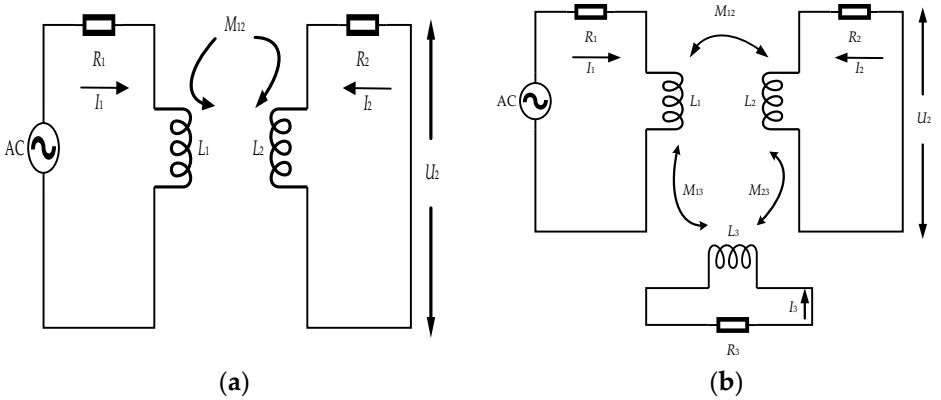

Figure 1. Equivalent circuits of probe: (**a**) without sample; (**b**) with sample.

From Figure 1a, the output voltage U_2 of the detection coil without sample is:

$$U_2 = Z_2 I_2 - j\omega M_{21} I_1, \tag{1}$$

where Z_2 is the impedance of the detection coil. According to the impedance formula, neglecting the capacitance due to the distribution of coil turns as follows:

$$Z_2 = R_2 + j\omega L_2, \tag{2}$$

From Figure 1b, the output voltage U_2 of the detection coil with sample is:

$$U_2 = Z_2 I_2 - j\omega M_{21} I_1 - j\omega M_{32} I_3, \quad (3)$$

where I_3 is the equivalent current of eddy currents induced in the sample by the coil, and M_{32} is the mutual inductance between the detection coil and the sample. From Equation (2), it can be observed that without a sample, the output voltage of the detection coil depends on the loop voltage after the coil generates the induced current and the voltage directly induced by the mutual inductance between the excitation coil and the detection coil. From Equation (3), the output voltage of the detection coil also includes the voltage generated by the mutual inductance M_{32} between the detection coil and the sample [22]. This part of the voltage signal can reflect defect information, which is the useful signal, while the voltage generated by the direct mutual inductance (M_{21}) between the excitation coil and the detection coil is considered the interference signal. If the interference signal is too strong, it may cause the effective signal to be submerged in noise, thereby reducing the detection sensitivity.

In conclusion, in order to achieve the signal processing function of eddy current testing equipment and improve its sensitivity, it is necessary to reduce interference signals and increase useful signals. This means reducing the voltage generated by the direct mutual inductance between the excitation coil and the detection coil while increasing the voltage generated by the mutual inductance between the detection coil and the CFRP sample.

2.2. Probe Design

2.2.1. Probe Geometry

Based on the above analysis, reducing the direct mutual inductance between the excitation coil and the detection coil while increasing the detection voltage can effectively improve the probe's sensitivity. Therefore, a novel triple rectangular coil probe was designed. The geometric structure of the probe is shown in Figure 2, which consists of three rectangular coils. One rectangular coil is used and placed horizontally as the detection coil, while two vertically placed rectangular coils are arranged side by side as the excitation coils, forming the novel triple rectangular coil probe. Using two rectangular coils as excitation coils can increase the induced eddy currents in the vertical direction within the sample, thereby increasing the detection voltage signal. In this configuration, the excitation coils and the detection coil are spatially perpendicular, effectively reducing the mutual inductance between the excitation coils and the detection coil [23], thus reducing the interference signal.

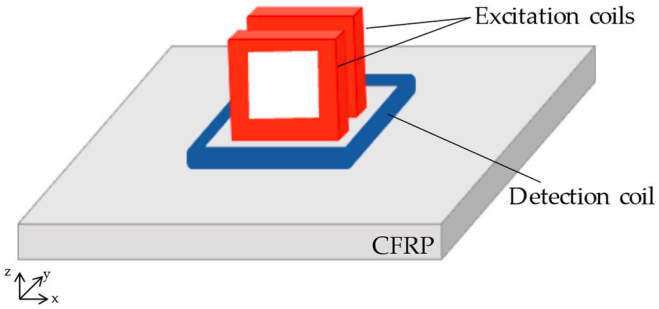

Figure 2. Novel triple rectangular coil probe.

In the detection process, the interference of delamination on the magnetic field manifests in the fact that defects will alter the eddy current paths within the CFRP sample. Therefore, when using dual-coil excitation, the direction of the excitation current flowing into the coils must also be considered. Figure 3 illustrates the eddy current paths in the sample under different excitation conditions. It can be observed that the presence of delamination blocks the original eddy current path. Moreover, from Figure 3b, it can be seen that

when opposite excitation currents are applied to the dual excitation coils, the eddy currents form a closed loop along the edge of the defect. Considering the geometry of the probe shown in Figure 2, the position of the detection coil is precisely above this loop. Therefore, the detection coil can effectively capture the delamination information in this configuration. Consequently, in subsequent studies, opposite excitation currents will be applied to the dual excitation coils.

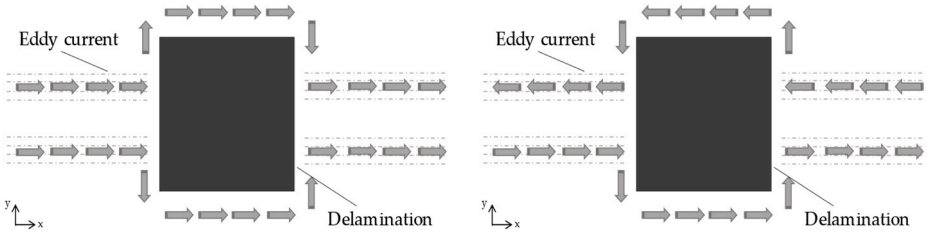

(**a**) (**b**)

Figure 3. Eddy current path in the CFRP sample under different excitations: (**a**) the current direction in the two excitation coils is same; (**b**) the current direction in the two excitation coils is opposite.

2.2.2. Probe Parameter Determination Method

Coil size directly affects the results of CFRP eddy current testing [24]. Generally, smaller coils have higher spatial resolution and better sensitivity to small defects (such as cracks). However, overly small coils can result in weak detection signals, which may drown out the defect signal in noise, ultimately leading to the inability to obtain useful defect information. Larger coils can generate deeper eddy current penetration depths, which are advantageous for detecting larger defects (such as delamination). However, excessively large coils during scanning may lead to significant differences between the detected defect edges and the actual defect edges, thereby increasing the difficulty in detecting defect edges. This study aims to design a probe with high sensitivity specifically for delamination. Therefore, it is necessary to comprehensively consider coil size to determine a set of suitable probe parameters.

The orthogonal experiment is a research method for studying multiple factors and levels of experiments. It can comprehensively and effectively explore the influence of multiple factors on a relatively small experimental scale [25]. When conducting an orthogonal experiment, first identify the factors and levels to be studied, and then select an appropriate orthogonal array to design the experimental plan. During the experiment, different levels of each factor are combined into experimental conditions and grouped according to the orthogonal array to ensure that each level of each factor appears in a relatively equal proportion with every level of other factors. Next, execute the experiments one by one according to the experimental plan, recording the experimental results for each group of conditions. Finally, evaluate the influence of each factor on the target variable using statistical analysis methods and determine the optimal combination of factors to achieve the optimization goals. In the process of determining probe parameters, there are many influencing factors. To reduce the number of blind tests and improve experimental efficiency, orthogonal experimental methods and finite element analysis are used to determine the probe parameters.

To ensure the orthogonality of the experiment, the number of levels for each factor is typically chosen as 2 m, where m is a positive integer. To assess the influence of each factor on the evaluation criteria, range analysis is conducted on the results of orthogonal experiments. This involves calculating the average value A_{ZJ} and the range T_Z:

$$A_{ZJ} = \frac{\sum_{i=1}^{n} y_{Zi}}{m}, \tag{4}$$

$$T_Z = R_{\mathrm{max}z} - R_{\mathrm{min}z}, \tag{5}$$

where i is the test number, Z is the influencing factor, N is the number of levels in the orthogonal experiment, J = 1, 2, ... N, y is the evaluation index, and n is the number of experiments. R_{maxZ} = max $\{A_{Z1}, A_{Z2} \ldots\ldots A_{ZJ}\}$, R_{minZ} = min $\{A_{Z1}, A_{Z2} \ldots\ldots A_{ZJ}\}$.

The range T_Z can be used to analyze the degree of influence of each factor on the evaluation criterion. The larger the T_Z, the more significant the influence of factor Z on the evaluation criterion [26]. In the range analysis, the average value A_{ZJ} when J = 1, 2, ... N describes the effect of the factor Z on the test result. By selecting a reference factor X (with no need to set levels) and considering its extreme values as the benchmark for the experiment, we can test whether other factors have a significant impact on the evaluation criterion. If the extreme value of a certain factor exceeds the extreme value of X, it indicates that this factor has a significant impact on the evaluation criterion, thereby validating the rationality of the designed experiment [27]. Finally, the number of levels with the largest A value for every factor is selected to achieve the experimental goal.

Considering the geometric structure of the probe, the parameters of the excitation coils will affect the parameters of the detection coil. Therefore, in the process of determining the parameters, the parameters of the excitation coils are prioritized. Furthermore, to ensure the uniformity of the generated magnetic field, the dual excitation coils use the same set of parameters.

1. Determination method of excitation coil parameters;

The magnetic flux density not only affects the generation of eddy currents but also directly relates to the distribution and intensity of the eddy currents in the conductor [28]. A higher magnetic flux density can make the changes in the detection signal caused by defects more significant, thereby affecting the detection sensitivity. Therefore, in the determination of the excitation coil parameters, the magnetic flux density (B) at a fixed point in the CFRP sample is chosen as the evaluation criterion, and the y in Equation (4) is replaced by the magnetic flux density (B). The relationship between the excitation coil size, the distance between the two excitation coils, and the magnetic flux density is studied. By changing the coil parameters, the magnetic flux density is indirectly controlled. The objective function for excitation coil parameter determination is shown as follows:

$$maxB(D_e, H_e, K_e, S_e, N_e), \tag{6}$$

where B represents the magnetic flux density, D_e is the width of the excitation coil winding, H_e is the height of the excitation coils, K_e is the thickness of the excitation coil bundle, S_e is the distance between the two excitation coils, and N_e is the number of turns in the excitation coils.

2. Determination method for detection coil parameters.

After determining the parameters of the excitation coils, it is necessary to choose a suitable evaluation criterion to determine the parameters of the detection coil. This involves applying an alternating current to the excitation coils of a known size to induce a magnetic field in the CFRP sample. Following this, the impact of changes in detection coil parameters on the evaluation criterion will be studied. The detection voltage change rate is used to represent the relative change between the voltage signal when delamination is present in the CFRP sample and when there is no delamination present. It is a normalized value, and a higher detection voltage change rate indicates a more significant relative change between the voltage signals with and without delamination. This means that the probe is more sensitive to delamination. Therefore, in the determination of the detection coil parameters, the detection voltage change rate (C) is selected as the evaluation criterion, and the y in Equation (4) is replaced by the rate of change of the detection voltage difference C. This implies selecting a representative delamination and detecting it with detection coils of different sizes to study the influence of various factors of the detection coils on the voltage

detection change rate of this defect. The equation for calculating the voltage detection change rate is as follows:

$$C = \frac{V_{\text{defect}} - V_{\text{nodefect}}}{V_{\text{nodefect}}}, \tag{7}$$

where V_{defect} is the voltage measured by the detection coil when there is a delamination, and V_{nodefect} is the voltage measured by the detection coil when there is no delamination.

The objective function for determining the detection coil parameters is shown in Equation (8):

$$maxC(D_{\text{r}}, H_{\text{r}}, K_{\text{r}}, N_{\text{r}}), \tag{8}$$

where D_{r} is the width of the detection coil, H_{r} is the height of the detection coil, K_{r} is the thickness of the detection coil winding, and N_{r} is the number of turns of the detection coil.

3. Finite Element Modeling and Probe Parameter Determination

3.1. Finite Element Model

In order to determine the parameters of the designed probe and validate its performance, this study utilizes COMSOL Multiphysics. Within the AC/DC module, the magnetic field was chosen as the physical field to establish a three-dimensional model for the novel embedded triple rectangular array probe detecting CFRP. Figure 4 shows the geometric model, which consists of three parts: the outermost rectangular air domain, the novel triple rectangular coil probe, and the CFRP sample. The geometric dimensions of the rectangular air domain are 300 mm × 300 mm × 100 mm. Figure 5 depicts the CFRP sample, which is composed of 16 layers of orthogonally laid carbon fiber composite material. The dimensions of the sample are 150 mm × 100 mm × 4 mm, with each layer having a thickness of 0.25 mm. The layup direction is $[0°/90°]_8$.

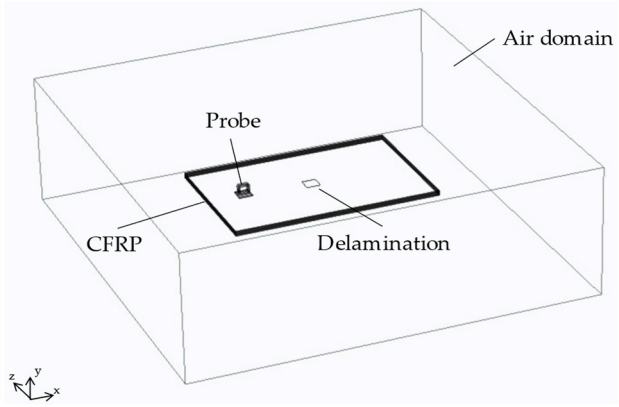

Figure 4. Geometric model.

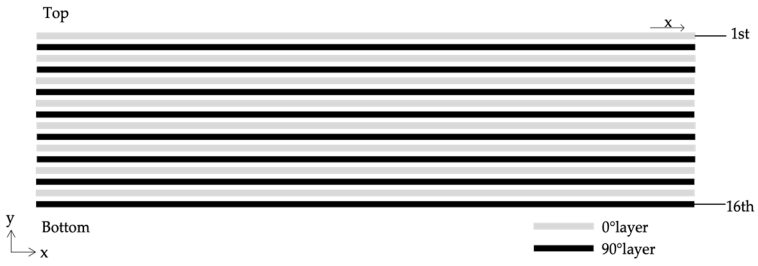

Figure 5. CFRP sample.

The electrical conductivity of CFRP exhibits significant anisotropy, meaning it has different conductivities in different directions. The conductivity tensor includes longitudinal conductivity (the fiber direction), transverse conductivity (perpendicular to the fiber direction), and interlayer conductivity. Specifically, the longitudinal conductivity (σ_{L}) is typically between 5000 S/m and 50,000 S/m, the transverse conductivity (σ_{T}) is between

10 S/m and 100 S/m, and the interlayer conductivity (σ_{cp}) is between 10 S/m and 100 S/m. It is generally considered that the interlayer conductivity is half of the transverse conductivity [29]. In the modeling, classic conductivity values (σ_L, σ_T, σ_{cp}) = (10,000, 100, 50) S/m were assigned to the CFRP. In the magnetic field, apart from electrical conductivity, other major material properties include relative magnetic permeability and relative permittivity. In this model, both relative magnetic permeability and relative permittivity are set to 1. The material for the coils is copper, with an electrical conductivity of 5.998×10^7 S/m. The conductivity of delamination and air is 0 S/m.

To balance computation accuracy and the computational capacity of the computer, different division methods are applied to various sections of the model. The air domain of the model is divided using refined tetrahedral mesh elements. The CFRP sample and the probe are divided using finer hexahedral mesh elements. The delamination part, which has the most significant impact on the solution results, is divided using highly refined hexahedral mesh elements. The boundary between the delamination and CFRP is divided using refined triangular mesh elements. After completing the mesh division, this model generates a total of 188,299 domain elements, 19,944 edge elements, and 160 vertex elements. The mesh partition of the simulation model is shown in Figure 6.

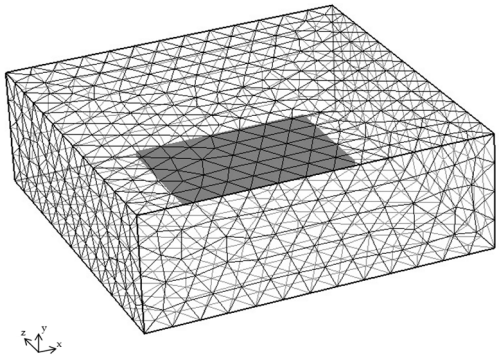

Figure 6. Mesh generation.

The equation for calculating the skin depth of the CFRP sample with an orthogonal ply orientation $[0°/90°]_8$ is [30]:

$$\delta = 2\sqrt{\frac{1}{\mu_0 \sigma_L \omega}}, \tag{9}$$

where ω is the angular frequency, μ_0 is the material's permeability, and σ_L is the fiber direction conductivity. The thickness of the sample in Figure 5 is 4 mm. According to Equation (9), the excitation frequency is determined to be 1 MHz. At this frequency, the skin depth is 7.1 mm, and eddy currents can penetrate to the bottom of the sample without significant attenuation. This is advantageous for detecting subsurface defects located deeper within the sample. Hence, in the simulation experiment, a sinusoidal current with a frequency of 1 MHz and amplitude of 1 A, in opposite directions, is applied to the two excitation coils. The control equation is shown as Equation (10):

$$j\omega\sigma A + \mu^{-1}\nabla \times \nabla \times A + \sigma\nabla\phi = J_e \tag{10}$$

where j is the imaginary unit, σ and μ are the conductivity tensor and relative permeability of the CFRP sample, J_e is the external excitation current density, A is the vector magnetic field at a point in space, and ϕ is the scalar electric potential.

When performing eddy current detection simulation using the aforementioned model for CFRP, the excitation coils generate an induced magnetic field in the sample, forming eddy currents as shown in Figure 3b. When delamination exists in the sample, it obstructs the path of the eddy currents. At this point, the field induced by the excitation coil undergoes changes. The detection coil can sense these changes in the excitation field, which can be reflected in its voltage readings. Recording the changes in voltage values in

the simulation can thus capture the characteristics of the field being measured. Figure 7 shows the scanning path for delamination detection. The novel triple rectangular coil probe scans from x = −50 mm along the positive x-axis to x = 50 mm, with a scanning step of 1 mm. In the simulation analysis, the detection voltage signals from the novel triple rectangular coil probe at each scanning point in the above scan process will be solved and recorded separately.

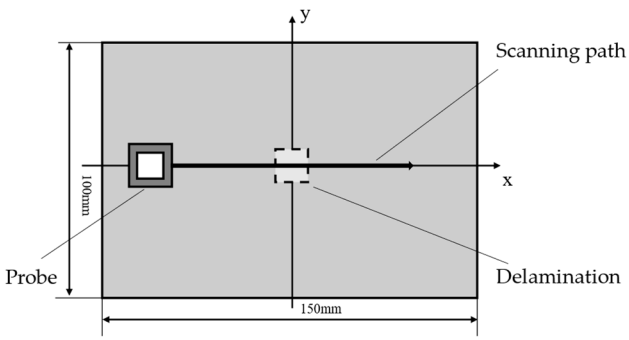

Figure 7. Delamination detection scanning path.

3.2. Determination of Probe Parameters

3.2.1. Determination of Excitation Coil Parameters

The design of an orthogonal experiment mainly considers the factors of the experiment and the levels of each factor. According to the previous analysis, the factors that need to be determined for the excitation coils are D_e, H_e, K_e, S_e, and N_e. According to the skin effect, in high-frequency AC circuits, current does not flow evenly across the entire cross-section of the conductor but instead concentrates more near the surface. To ensure stable efficiency in signal transmission, when making coils, keeping the wire radius smaller than the skin depth at the excitation frequency can effectively increase the current density within the wire cross-section, reduce resistance, and thereby ensure probe performance. The coil winding wire usually requires copper-enamel wire with a diameter of 0.2 mm or less. In this study, the selected excitation frequency is 1 MHz, and at this frequency, the skin depth of copper wire is 0.06 mm. Therefore, choose a copper-enamel wire with a diameter of 0.1 mm to wind the probe. After the wire diameter is determined, the relationship between N_e, H_e, and K_e is as follows:

$$K_e H_e = 0.01 N_e \tag{11}$$

Therefore, in the orthogonal experiment, only four independent factors need to be considered (D_e, H_e, K_e, and S_e). The simplified objective function is as follows:

$$maxB(D_e, H_e, K_e, S_e) \tag{12}$$

In order to comprehensively and effectively understand the primary and secondary effects of each factor with as few experimental trials as possible, an orthogonal experiment with four (2^2) levels is chosen for each factor in the process of determining coil parameters. The lateral dimensions of delamination are typically above 10 mm, making them relatively large defects. Therefore, slightly larger excitation coils should be chosen to induce a larger magnetic field inside the CFRP sample. Specifically, the inner diameter of the excitation coils should be greater than half of the lateral dimensions of the delamination. However, if the coil size is too large, it can indeed affect the sensitivity of the probe. This means that when the defect size changes, the probe may not be as sensitive to those changes. Therefore, the selected four levels need to cover the characteristics of both large and small coils to achieve a comprehensive and systematic study of coil parameters, thus achieving the design objectives. The four levels chosen for each factor are shown in Table 1.

Table 1. Factors and levels of orthogonal tests of excitation coils.

Impact Factors	Level 1	Level 2	Level 3	Level 4
D_e/mm	2	4	6	8
H_e/mm	0.6	0.8	1	1.2
K_e/mm	0.6	0.8	1	1.2
S_e/mm	1	2	3	4

To validate the rationality of the experiment, *X*e is chosen as the reference factor to conduct a 4-factor 4-level orthogonal experiment L16 (4^4), which requires a total of 16 trials. That is, simulation detection was carried out on the CFRP sample shown in Figure 5 under different parameter combinations of the excitation coils, analyzing and studying magnetic flux density at the point on the sample surface directly beneath the probe. The results are shown in Table 2.

Table 2. Orthogonal experiment table for the excitation coils.

NO.	Evaluated Parameters				Reference	Results
	D_e/mm	H_e/mm	K_e/mm	S_e/mm	X_e	*B*/T
#1	2	0.6	0.6	1	X_{e1}	0.00593
#2	2	0.8	0.8	2	X_{e2}	0.00765
#3	2	1	1	3	X_{e3}	0.00772
#4	2	1.2	1.2	4	X_{e4}	0.00308
#5	4	0.6	0.8	3	X_{e4}	0.00836
#6	4	0.8	0.6	4	X_{e3}	0.00437
#7	4	1	1.2	1	X_{e2}	0.01468
#8	4	1.2	1	2	X_{e1}	0.01538
#9	6	0.6	1	4	X_{e2}	0.00669
#10	6	0.8	1.2	3	X_{e1}	0.01538
#11	6	1	0.6	2	X_{e4}	0.01227
#12	6	1.2	0.8	1	X_{e3}	0.01474
#13	8	0.6	1.2	2	X_{e3}	0.01156
#14	8	0.8	1	1	X_{e4}	0.01361
#15	8	1	0.8	4	X_{e1}	0.00956
#16	8	1.2	0.6	3	X_{e2}	0.01054
A_{Z1}	0.00609	0.00813	0.00828	0.01224	0.01156	
A_{Z2}	0.01070	0.01025	0.01008	0.01171	0.00989	
A_{Z3}	0.01227	0.01106	0.01085	0.01050	0.00960	
A_{Z4}	0.01132	0.01094	0.01118	0.00592	0.00933	
T_Z	0.00617	0.00292	0.00289	0.00578	0.00167	

In Table 2, the T_Z of each factor is greater than the T_Z of the reference factor X_e. This indicates that each factor at the selected levels has a significant effect on magnetic flux density, proving the rationality of the experiment. The influence of the four factors on magnetic flux density is: $D_e > S_e > H_e > K_e$. According to the experimental results in Table 2, the number of levels with the largest A value for every factor is selected to increase the magnetic flux density and consequently enhance the signal amplitude in the sample. Thus, the combination $D_{e3}H_{e3}K_{e4}S_{e1}$ is determined by the geometry parameters of the excitation coils.

3.2.2. Determination of Detection Coil Parameters

The designed probe is aimed at detecting delamination with sizes ranging from 10 mm to 30 mm and thicknesses between 0.05 mm and 0.15 mm. This size range is commonly encountered for delamination, demonstrating a certain level of generality [31,32]. Therefore, when determining the parameters of the detection coil, we chose to simulate the detection of a delamination with dimensions of 15 mm × 15 mm × 0.1 mm, which represents a size that is relatively central within the range. That means an alternating current is applied to the excitation coils with the parameter combination of $D_{e3}H_{e3}K_{e4}S_{e1}$ in Table 2, and simulation

detection is conducted on the CFRP sample as shown in Figure 5. The sample contains a delamination with dimensions of 15 mm × 15 mm × 0.1 mm. The study will investigate the impact of detection coil size on the rate of change in detection voltage. The factors that need to be determined for the detection coil are D_r, H_r, K_r, and N_r. Similar to the excitation coil, the detection coil also uses enameled wire with a diameter of 0.1 mm for winding. Therefore, in the orthogonal experiment, only three independent factors need to be considered (D_r, H_r, and K_r), and the objective function is as shown in Equation (13):

$$maxC(D_r, H_r, K_r) \tag{13}$$

Similar to the excitation coil, in the process of determining the parameters of the detection coil, an orthogonal experiment with four (2^2) levels is chosen for each factor. Considering the geometric structure of the probe, the width of the detection coil winding must be larger than the outer diameter of the excitation coils. To ensure that the detection coil extracts a sufficiently large signal and is not overwhelmed by noise, the selection of four levels for each factor of the detection coil is based on the orthogonal experimental results of the excitation coils. This means that the selection is made by slightly expanding the range based on the outer diameter of the excitation coils. The four levels chosen for each factor of the detection coil are shown in Table 3.

Table 3. Factors and levels of orthogonal tests of the detection coil.

Impact Factors	Level 1	Level 2	Level 3	Level 4
D_r/mm	9	10	11	12
H_r/mm	0.6	0.8	1	1.2
K_r/mm	0.6	0.8	1	1.2

X_r is chosen as the reference factor. An orthogonal experiment with three factors and four levels, L16 (3^4), is conducted, requiring a total of 16 trials. The results are shown in Table 4.

Table 4. Orthogonal experiment table for detection coil.

NO.	Evaluated Parameters			Reference	Results
	D_r/mm	H_r/mm	K_r/mm	X_r	C
#1	9	0.6	0.6	X_{r1}	0.05874
#2	9	0.8	0.8	X_{r2}	0.05785
#3	9	1	1	X_{r3}	0.05762
#4	9	1.2	1.2	X_{r4}	0.05683
#5	10	0.6	0.8	X_{r3}	0.05396
#6	10	0.8	0.6	X_{r4}	0.05547
#7	10	1	1.2	X_{r1}	0.05259
#8	10	1.2	1	X_{r2}	0.05774
#9	11	0.6	1	X_{r4}	0.04989
#10	11	0.8	1.2	X_{r3}	0.04877
#11	11	1	0.6	X_{r2}	0.05067
#12	11	1.2	0.8	X_{r1}	0.04972
#13	12	0.6	1.2	X_{r2}	0.04260
#14	12	0.8	1	X_{r1}	0.04622
#15	12	1	0.8	X_{r4}	0.04649
#16	12	1.2	0.6	X_{r3}	0.04684
A_{Z1}	0.03340	0.05130	0.05293	0.05182	
A_{Z2}	0.05494	0.05208	0.05201	0.05222	
A_{Z3}	0.04976	0.05184	0.05287	0.05180	
A_{Z4}	0.04554	0.05278	0.05020	0.05217	
T_Z	0.02153	0.00148	0.00273	0.00041	

In Table 4, the T_Z of each factor is greater than the T_Z of the reference factor X_r. This indicates that each factor at the selected levels has a significant effect on the detection voltage change rate, proving the rationality of the experiment. By comparing the range T_Z, we can analyze the extent to which each factor affects the detection voltage change rate. A larger T_Z indicates a more significant influence of factor Z on the evaluation metric. Based on the T_Z values in Table 4, it can be seen that D_r is the primary factor, while H_r and K_r are secondary factors. The number of levels with the largest A value for every factor is selected to enhance the rate of change in detection voltage. Thus, the combination $D_{r2}H_{r4}K_{r3}$ is determined as the geometry parameters of the detection coil.

In summary, the parameters of the excitation coils and detection coil have been determined, as shown in Table 5.

Table 5. Probe parameters.

Probe Parameters	Excitation CoilParameters					Detection Coil Parameters			
	D_e/mm	H_e/mm	K_e/mm	N_e	S_e/mm	D_r/mm	H_r/mm	K_r/mm	N_r
	6	1	1.2	120	1	10	1.2	1	120

4. Simulation Analysis of the Designed Probes

4.1. Analysis of Probe Scanning Modes

In the process of manufacturing CFRP, different fiber orientations can be defined manually according to specific requirements. The electrical conductivity varies in different directions, resulting in different eddy current distributions. Taking the CFRP sample with an orthogonal ply layup as shown in Figure 5 as an example, analyze the eddy current distribution in the multi-directional laminate through simulation. Figure 8 shows the eddy current distribution in different layers of the CFRP sample as depicted in Figure 5 when the center of the designed probe is located at x = y = 0. Here, (a) and (c) represent the eddy current distribution in the first layer of the sample (fiber direction 0°) and the third layer (fiber direction 0°), respectively, while (b) and (d) represent the eddy current distribution in the second layer (fiber direction 90°) and the fourth layer (fiber direction 90°), respectively.

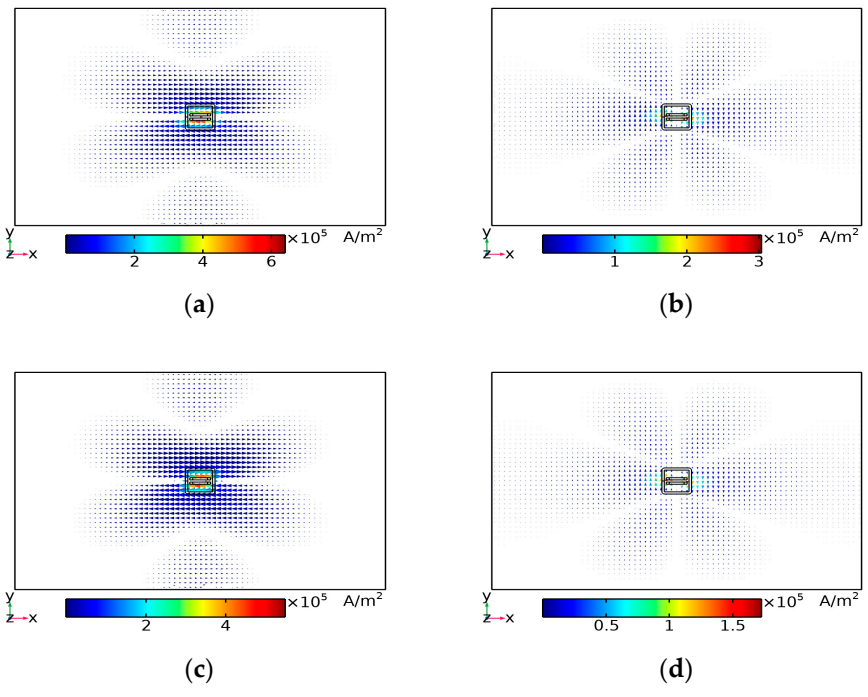

Figure 8. Eddy current distribution in CFRP sample: (**a**) first layer (0°); (**b**) second layer (90°); (**c**) third layer (0°); (**d**) fourth layer (90°).

The arrows in Figure 8 represent the distribution of eddy currents inside the sample, with denser arrows indicating a more concentrated eddy current presence. Based on the distribution of eddy currents shown in the diagram and the magnitude of the eddy current density, it can be observed that in the layers where the fiber direction is 0°, the eddy currents exhibit a tendency to flow along the X-axis. In this case, the fiber direction is the same as the direction of the excitation current, resulting in a larger and more concentrated eddy current induced in the sample. On the other hand, in the layers where the fiber direction is 90°, the eddy currents tend to flow along the Y-axis. Here, the fiber direction is different from the direction of the excitation current, leading to smaller and relatively more dispersed eddy currents induced in the sample. Therefore, eddy currents tend to concentrate in layers where the excitation current direction is the same as the fiber direction. However, the distribution of eddy current directly affects the magnetic field distribution in the CFRP sample and the effectiveness of defect detection [33,34]. When defects are located in layers where the excitation current direction is the same as the fiber direction, the detection effectiveness is better. Conversely, when defects are located in layers where the excitation current direction is different from the fiber direction, the detection effectiveness may be relatively poorer.

For the above-mentioned problem, this paper proposes two probe scanning modes, as shown in Figure 9. When using scanning mode 1 for eddy current testing, the excitation current direction is along the x-axis. In this case, the eddy currents in the sample are concentrated in the layers where the fiber direction is parallel to the x-axis, i.e., the 0° layer, as shown in Figure 5. When using scanning mode 2, the excitation current direction is along the y-axis. In this case, the eddy currents in the sample are concentrated in the layers where the fiber direction is parallel to the y-axis, i.e., the 90° layer, as shown in Figure 5.

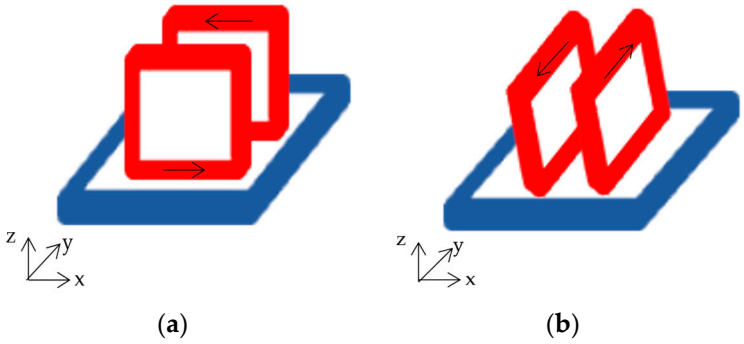

(**a**) (**b**)

Figure 9. Probe scanning modes: (**a**) scanning mode 1; (**b**) scanning mode 2.

To gain a clearer understanding of the detection of delamination under two scanning modes of the probes, the eddy current distributions in the orthogonal laminated CFRP specimen shown in Figure 5 were simulated for the two aforementioned modes. Figure 10 shows the current density models in the x-z plane of the sample under both scanning modes. It is evident from Figure 10 that layers aligned with the excitation current direction exhibit higher current density models, consistent with the conclusions from Figure 8. Based on this, the impact of delamination on the eddy currents within the CFRP sample under different scanning modes was simulated. Figures 11 and 12 illustrate the effects of delamination on the eddy currents in the CFRP sample under the two scanning modes.

As shown in Figures 11a and 12a, different probe placements result in different induced electromagnetic fields within the CFRP sample, leading to varying eddy current distributions. In Figures 11b and 12b, a distinct area of almost zero current can be observed, indicating that delamination significantly hinders the eddy currents in the CFRP under both scanning modes, causing a redistribution of the original magnetic field. By comparing the numerical values of the current density models with and without delamination in the CFRP sample, it can be observed that the presence of delamination causes a decrease in the

current values within the CFRP sample. This change can be reflected in the voltage values of the detection coils.

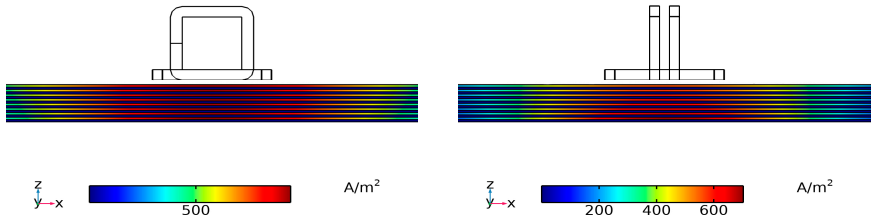

(**a**) (**b**)

Figure 10. Current density in CFRP x-z plane: (**a**) scanning mode 1; (**b**) scanning mode 2.

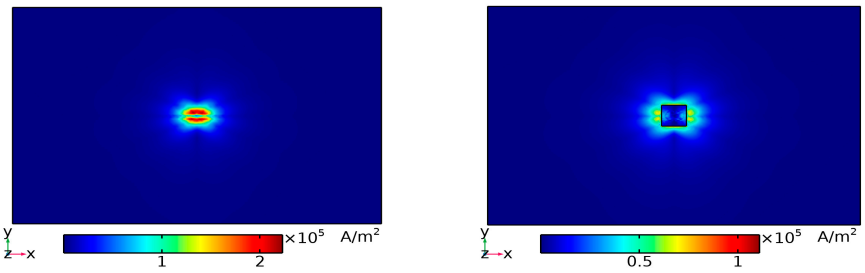

(**a**) (**b**)

Figure 11. Current density in CFRP x-y plane under scanning mode 1: (**a**) without delamination; (**b**) with delamination.

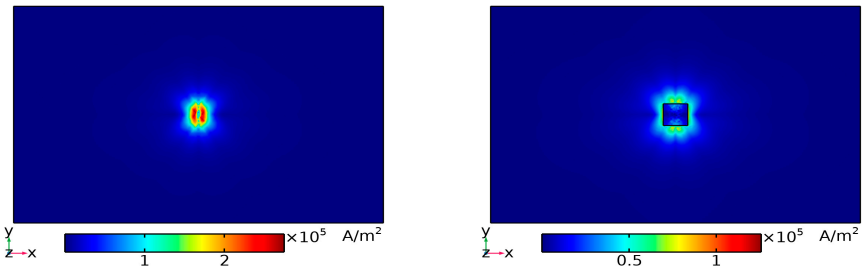

(**a**) (**b**)

Figure 12. Current density in CFRP x-y plane under scanning mode 2: (**a**) without delamination; (**b**) with delamination.

To demonstrate the effectiveness of the above modes, simulation detection was performed on the orthogonal layup CFRP sample, as shown in Figure 5, using the two aforementioned approaches. Each simulation experiment included setting a delamination with dimensions of 10 mm × 10 mm × 0.1 mm in different layers of the CFRP sample. Table 6 shows the results of the detection voltage change rate.

Table 6. Results of delamination with different probe scanning modes.

Delamination Location	*C*	
	Scanning Mode 1	Scanning Mode 2
Layer 2 (90°)	0.01934	0.05480
Layer 4 (90°)	0.01492	0.03510
Layer 6 (90°)	0.00838	0.02555
Layer 3 (0°)	0.03847	0.00946
Layer 5 (0°)	0.02748	0.00707
Layer 7 (0°)	0.02185	0.00595

From the detection results in Table 6, it can be seen that when using scanning mode 1 for eddy current testing, when the excitation current direction is aligned with the fiber direction (0° layer), C is relatively high. For example, the maximum C value is 0.03847 for the third layer (0° layer). Similarly, when using scanning mode 2 for eddy current testing, when the excitation current direction is aligned with the fiber direction (90° layer), C is also relatively high. For example, the maximum C value is 0.05480 for the second layer (90° layer). This result validates the effectiveness of the probe scanning modes illustrated in Figure 9.

4.2. Simulation Analysis of Delamination Eddy Current Testing

The presence of delamination changes the path and distribution of eddy currents, resulting in changes in the detection voltage, which reflects information about defects within the CFRP sample. To comprehensively explore the detection capabilities of the designed probes for delamination, various delaminations were introduced into the simulation experiments conducted in CFRP samples (Figure 5) with orthogonal laminations. The designed probes were used to simulate detection for delamination of different dimensions and were positioned at various locations within the CFRP sample. The relevant parameters of the probe for the above simulation experiments are summarized in Table 7.

Table 7. Probe parameters summary.

Name	Parameter
D_e (excitation coils)	6 mm
H_e (excitation coils)	1 mm
K_e (excitation coils)	1.2 mm
S_e (excitation coils)	1 mm
N_e (excitation coils)	120
D_r (detection coil)	10 mm
H_r (detection coil)	1 mm
K_r (detection coil)	1.2 mm
N_r (detection coil)	120
lift-off distance	0.5 mm
excitation frequency	1 MHz
excitation current	1 A

4.2.1. Simulation Analysis of Eddy Current Testing for Delamination of Various Dimensions

In the simulation experiments, the delamination was located in the third layer (0° layer) of the CFRP sample shown in Figure 5, with the defect centers at x = y = 0. The specific defect parameters are shown in Tables 8 and 9. Eddy current testing was conducted through simulation of the delamination of different lateral dimensions and different thicknesses.

Table 8. Different lateral dimensions delamination parameters.

Delamination Number	Delamination Parameter	Delamination Location
Delamination 1	10 mm × 10 mm × 0.1 mm	Layer 3 (0°)
Delamination 2	20 mm × 20 mm × 0.1 mm	Layer 3 (0°)
Delamination 3	30 mm × 30 mm × 0.1 mm	Layer 3 (0°)

Table 9. Different thickness delamination parameters.

Delamination Number	Delamination Parameter	Delamination Location
Delamination 4	15 mm × 15 mm × 0.05 mm	Layer 3 (0°)
Delamination 5	15 mm × 15 mm × 0.1 mm	Layer 3 (0°)
Delamination 6	15 mm × 15 mm × 0.15 mm	Layer 3 (0°)

Based on the previous analysis, the probe scanning mode shown in Figure 9a was selected for simulating the detection of delamination, scanning from both the top and bottom of the sample. The delamination detection results are shown in Figures 13 and 14. The signal variation curve shown in Figure 13 represents the curve of detection voltage difference changes obtained from top scanning, while Figure 14 shows the signal variation curves obtained from bottom scanning. Each point on the curve represents the voltage difference between when the probe detects the presence of a delamination in the CFRP sample along the scanning path shown in Figure 7 and when the probe detects no delamination in the CFRP sample. In the resulting figure, the center of the coil set is at the indicated probe position.

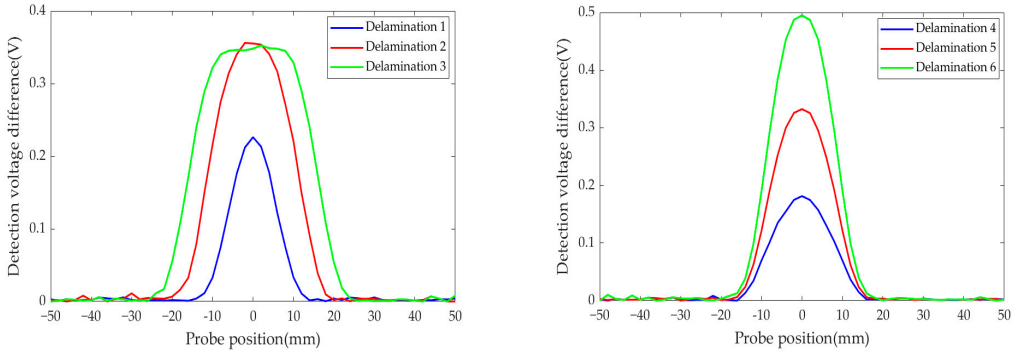

Figure 13. Detection voltage differences obtained from top scanning for different dimensions of delamination: (**a**) different lateral dimensions; (**b**) different thicknesses.

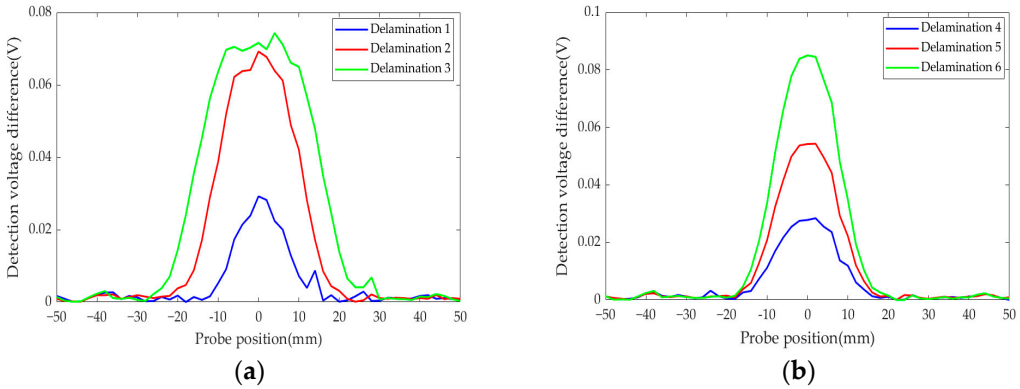

Figure 14. Detection voltage differences obtained from bottom scanning for different dimensions of delamination: (**a**) different lateral dimensions; (**b**) different thicknesses.

Comparing the detection results from Figures 13 and 14, it can be observed that the detection voltage difference obtained from top scanning is greater than that from bottom scanning. This is because when scanning defects in Tables 8 and 9 from the bottom, the defects are farther away from the probe. As a result, the eddy currents within the CFRP sample decrease with increasing thickness, leading to smaller detection signals.

From Figures 13a and 14a, it can be seen that for smaller lateral dimensions of delamination (Delamination 1 and 2), when the probe is directly above the delamination (x = 0 mm), the detection voltage difference reaches a peak. However, for larger lateral dimension delamination (Delamination 3), there is no peak in the detection voltage difference when the probe is directly above the delamination. This is because when the probe size differs significantly from the delamination dimension, it will reduce the probe's detection sensitivity to some extent. For delamination of different lateral dimensions, the relative position of the probe when the detection voltage difference rises and falls is different. The

larger the lateral dimension, the closer the probe's position is to the front when the detection voltage difference rises. Therefore, quantitative evaluation of the lateral dimension of delamination can be achieved by calculating the relative position of the probe when the detection voltage difference rises and falls.

From Figures 13b and 14b, it can be seen that the impact of different thicknesses of delamination on the detection voltage difference varies. When the thickness of the delamination is 0.05 mm, the detection voltage difference peak is the smallest, at 0.1814 V and 0.0284 V. As the thickness of the delamination increases, the peak detection voltage difference increases. When the delamination thickness is 0.15 mm, the detection voltage difference peak rises to 0.4950 V and 0.085 V. These results indicate that it is possible to quantitatively assess the thickness of the delamination by calculating the peak detection voltage difference during the detection process.

4.2.2. Simulation Analysis of Eddy Current Testing for Delamination of Various Locations

According to the analysis in Section 3.1, at the excitation frequency used in the simulation, the skin depth is 7.1 mm. In theory, defects smaller than this depth can be effectively detected. To investigate the detection effectiveness of the designed probe for subsurface defects located deeper within the CFRP sample, simulations were conducted with different delaminations of the same dimension at various locations in the CFRP sample (Figure 5). Table 10 provides the specific parameters of the delamination. Perform top scanning of defects inside the CFRP sample using the designed probes, canning mode 1 was used for defects in the 0° layer, while scanning mode 2 was used for defects in the 90° layer. The detection results are shown in Figure 15.

Table 10. Delamination at different locations.

Delamination Number	Delamination Parameter	Delamination Location
Delamination 7	15 mm × 15 mm × 0.1 mm	Layer 11 (0°)
Delamination 8	15 mm × 15 mm × 0.1 mm	Layer 12 (90°)
Delamination 9	15 mm × 15 mm × 0.1 mm	Layer 13 (0°)
Delamination 10	15 mm × 15 mm × 0.1 mm	Layer 14 (90°)
Delamination 11	15 mm × 15 mm × 0.1 mm	Layer 15 (0°)
Delamination 12	15 mm × 15 mm × 0.1 mm	Layer 16 (90°)

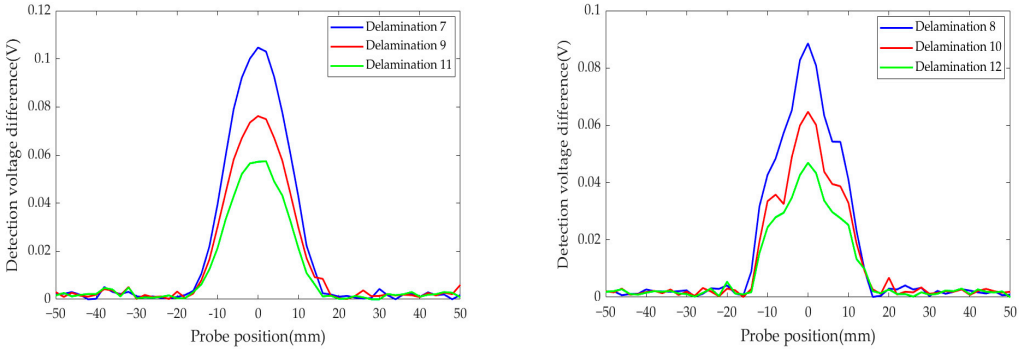

(a) **(b)**

Figure 15. Detection voltage difference for delamination at different locations: (**a**) scanning mode 1; (**b**) scanning mode 2.

According to Figure 15, it can be observed that the curves of the detection voltage differences obtained from different scanning modes exhibit differences. This is caused by the inherent characteristics of the probe [35]. The designed probe successfully detected subsurface defects located deeper within the sample. From the pattern of voltage difference changes, for defects of the same dimension, the closer the defect is to the top surface of the sample, the larger the detection voltage difference peak obtained from top scanning,

resulting in a better detection effect. According to the results of the simulation experiments, the designed probes can detect the delamination at the bottom layer (Layer16) of the CFRP sample (Figure 5).

4.2.3. Simulation Analysis of Eddy Current Testing for Multiple Delamination

In order to conduct a detailed analysis of the detection signals of the designed probe, the above simulation experiments only consider the simple case where there is only one layer inside the CFRP sample. In reality, CFRP can have delamination in different dimensions at different locations. To investigate the detection performance of the designed probe in this scenario, we conducted simulation experiments using the designed probe to simulate the detection of delamination of different dimensions and positions within the CFRP sample (Figure 5) with an orthogonal layup. The delamination dimensions and their corresponding layers are Delamination 1 from Table 8 and Delamination 12 from Table 10. The planar positions of the two defects are as shown in Figure 16, and the detection results are depicted in Figure 17.

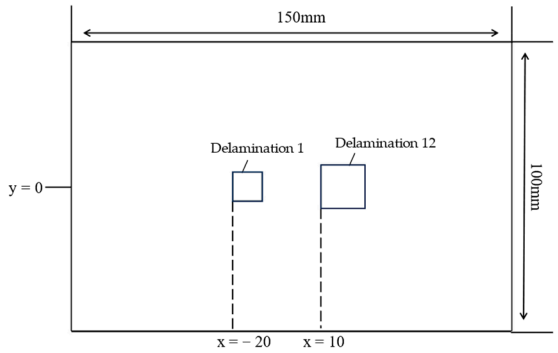

Figure 16. The planar positions of the multiple delaminations.

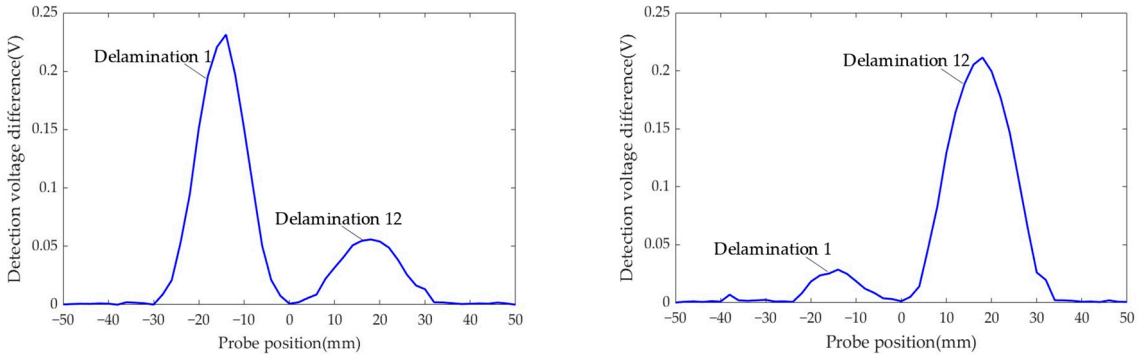

Figure 17. Detection voltage difference for multiple delamination: (**a**) top scanning; (**b**) bottom scanning.

Based on Figure 17, it is evident that the designed probe successfully detects delamination of different dimensions and locations within the CFRP sample during both top and bottom scans. However, due to the small distance between the two delaminations and the edge effect on the probe during scanning, it is challenging to determine the width of the delamination based solely on the relative positions of the rising and falling edges of the detection voltage difference. Instead, a rough estimate of the layer where the delamination is located can be made by combining the results from the top scanning with the peak detection voltage obtained from the bottom scanning.

4.3. Comparison Analysis of Different Probes

Figure 18 shows two commonly used probes for CFRP eddy current testing: the single pancake probe and the single rectangular probe. In the simulation experiments, these two probes, along with the designed probe, were used to detect the delamination in the CFRP sample (Figure 5). The dimensions and number of turns of the three probe excitation coils are the same. Figure 19 shows the detection voltage difference signals obtained by the three probes as they scanned the CFRP sample along the scanning path illustrated in Figure 7. The sample contains a delamination with dimensions of 15 mm × 15 mm × 0.1 mm.

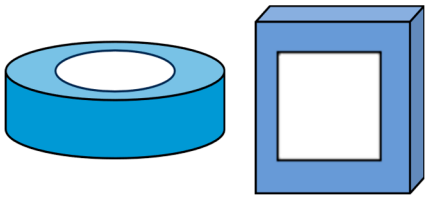

Figure 18. CFRP eddy current testing commonly used probe: (**a**) single pancake probe; (**b**) single rectangular probe.

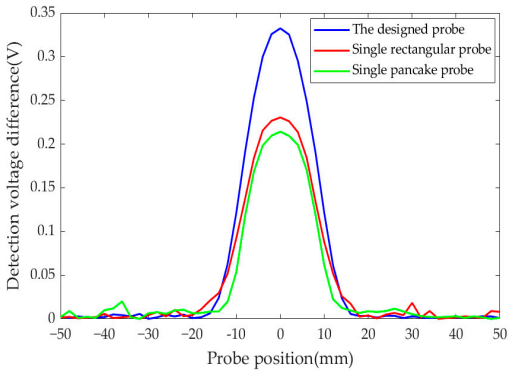

Figure 19. Detection voltage differences for different probes.

From Figure 19, it can be seen that the designed probe has a detection voltage difference peak of 0.3324 V. The detection voltage difference for the single rectangular probe is 0.2266 V, which is only 68% of the designed probe's detection voltage difference. The detection voltage difference peak for the single pancake probe is 0.2095 V, which is only 64% of the designed probe's detection voltage difference. It is evident that the designed probe has a larger detection voltage difference peak, making the detection signal less susceptible to being overwhelmed by noise in actual testing. When the dimensions and number of turns of the excitation coils for the three types of probes are the same, the designed probe exhibits stronger detection capability compared with the single rectangular and single pancake probes.

In order to visually compare the sensitivity of the three probes, each probe was used to simulate the detection of three different dimensions of delamination in the CFRP sample shown in Figure 5 (15 mm × 15 mm × 0.1 mm, 15 mm × 15 mm × 0.05 mm, and 10 mm × 10 mm × 0.05 mm). Calculate the changes in the detection voltage difference peak (V_{peak}) of the three probes with the changes in delamination lateral dimension (d) and delamination thickness (h). This calculation involves an approximate slope calculation:

$$Sensitivity1 = \frac{\Delta V_{\text{peak}}}{\Delta d} \tag{14}$$

$$Sensitivity2 = \frac{\Delta V_{\text{peak}}}{\Delta h} \tag{15}$$

The calculation results from Equation (14) reflect the sensitivity of the probe to changes in delamination lateral dimension, while the results from Equation (15) reflect the sensitivity of the probe to changes in delamination thickness. Through these calculations, the sensitivity of the probe can be comprehensively evaluated [36]. Table 9 presents the sensitivities of the three probes.

According to the results in Table 11, when the dimensions and number of turns of the excitation coils for the three types of probes are the same, the novel triple rectangular coil probe exhibits higher detection sensitivity for the defects set in the simulation experiment. When the lateral dimension of delamination changes by 5 mm, the sensitivity of the single pancake probe and the single rectangular coil probe is only 88.24% and 72.55% of that of the novel triple rectangular coil probe. Additionally, the novel triple rectangular coil probe is more sensitive to changes in delamination thickness. When the delamination thickness changes by 0.5 mm, the sensitivity of the single pancake probe and the single rectangular coil probe is only 49.04% and 56.69% of that of the novel triple rectangular probe.

Table 11. The sensitivities of different probes.

Probe Types	*Sensitivity* 1	*Sensitivity* 2
Single pancake probe	0.0090 (V/mm)	1.4809 (V/mm)
Single rectangular probe	0.0074 (V/mm)	1.7120 (V/mm)
Novel triple rectangular coil probe	0.0102 (V/mm)	3.0200 (V/mm)

5. Conclusions

This paper presents a novel triple rectangular coil probe designed for detecting CFRP delamination. The structure of this probe reduces the direct mutual inductance between the excitation coils and the detection coil, thereby minimizing the impact of interference signals. This design allows the detection coil to capture defect information to the greatest extent possible, thereby improving detection sensitivity and facilitating delamination inspection. The main conclusions are as follows:

(1) The designed probe has different scanning modes for CFRP samples with different layers. When the direction of the excitation current is consistent with the direction of the fibers, the detection effect of the delamination is optimal.

(2) The designed probes can sensitively detect delamination from both the top and bottom surfaces of the CFRP sample, including those located deeper within the sample. In the detection of delamination with different lateral dimensions, the relative position of the probe varies when the detection voltage difference rises and falls. The larger the lateral dimension, the further forward the probe's relative position during voltage difference rise and the further backward during voltage fall. By studying the relative position of the probe during voltage difference rise and fall, quantitative detection of the lateral dimension of delamination can be achieved. For delamination of different thicknesses, the size of the detection voltage difference peak varies. Through studying the detection voltage difference peaks that occur during the detection process, quantitative detection of the thickness of delamination can be achieved, providing valuable quantitative analysis references for CFRP delamination detection. For detecting multiple defects within the CFRP sample, the designed probes can successfully detect them, but determining the dimension of the defects based solely on their detection signals can be challenging. However, combining the results of top and bottom scans can provide a rough estimation of the dimension and location of the delamination.

(3) Under the condition where the dimensions and number of turns of the excitation coils are the same for all three probes, when the lateral dimension of delamination changes by 5 mm, the sensitivity of the single pancake probe and the single rectangular coil probe is only 88.24% and 72.55% of that of the novel triple rectangular coil probe. When the delamination thickness changes by 0.5 mm, the sensitivity of the single

pancake probe and the single rectangular coil probe is only 49.04% and 56.69% of that of the novel triple rectangular coil probe.

In conclusion, the probe proposed in this paper is feasible and effective for detecting CFRP delamination and meets the demand for high-sensitivity detection. This probe has guiding significance for the design and development of probes for CFRP delamination eddy current testing and provides valuable references for the quantitative evaluation of delamination in CFRP eddy current testing.

Author Contributions: Conceptualization, Y.Z. (Yingni Zhou) and B.Y.; methodology, Y.Z. (Yingni Zhou); software, Y.Z. (Yingni Zhou); validation, Y.Z. (Yingni Zhou), H.C., and B.Y.; formal analysis, Y.Z. (Yingni Zhou), Y.Z. (Yangkun Zou), and Z.Z.; investigation, Y.Z. (Yingni Zhou); resources, B.Y.; data curation, Y.Z. (Yingni Zhou) and H.X.; writing—original draft preparation, Y.Z. (Yingni Zhou); writing—review and editing, B.Y.; visualization, B.Y.; supervision, B.Y.; project administration, B.Y.; funding acquisition, B.Y. All authors have read and agreed to the published version of the manuscript.

Funding: This research was funded by the Yunnan Fundamental Research Projects, grant number 202301AS070052. This research was funded by the Young and Middle-Aged Academic and Technical Leaders Reserve Talents Project of Yunnan Province, grant number 202305AC160062.

Institutional Review Board Statement: Not applicable.

Informed Consent Statement: Not applicable.

Data Availability Statement: Data are contained within the article.

Conflicts of Interest: The authors declare no conflict of interest.

References

1. Cheng, J.; Qiu, J.H.; Xu, X.J.; Ji, H.L.; Takagi, T.; Uchimoto, T. Research advances in eddy current testing for maintenance of carbon fiber reinforced plastic composites. *Int. J. Appl. Electrom.* **2016**, *51*, 261–284. [CrossRef]
2. Gong, W.R.; Chen, J.L.; Patterson, E.A. Buckling and delamination growth behaviour of delaminated composite panels subject to four-point bending. *Compos. Struct.* **2016**, *138*, 122–133. [CrossRef]
3. Krishnamoorthy, A.; Boopathy, S.R.; Palanikumar, K. Delamination analysis in drilling of CFRP composites using response surface methodology. *J. Compos. Mater.* **2009**, *43*, 2885–2902. [CrossRef]
4. Carpenter, D.C. Use of the finite element method in simulation and visualization of electromagnetic nondestructive testing applications. *Mater. Eval.* **2000**, *58*, 877–881.
5. Lu, Q.Y.; Wong, C.H. Applications of non-destructive testing techniques for post-process control of additively manufactured parts. *Virtual Phys. Prototyp.* **2017**, *12*, 301–321. [CrossRef]
6. Han, S.L.; Li, Q.Z.; Cui, Z.; Xiao, P.; Miao, Y.N.; Chen, L.; Li, Y. Non-destructive testing and structural health monitoring technologies for carbon fiber reinforced polymers: A review. *Nondestruct. Test. Eval.* **2024**, 1–37. [CrossRef]
7. Meng, M.; Chua, Y.J.; Wouterson, E.; Ong, C.P.K. Ultrasonic signal classification and imaging system for composite materials via deep convolutional neural networks. *Neurocomputing.* **2017**, *257*, 128–135. [CrossRef]
8. Caliskan, U.; Yildiz, F.; Teke, S.; Ozdemir, A.T. Impact-delamination detection in repaired-composite laminates using numerical and ultrasonic method. *J. Nondestruc. Eval.* **2022**, *41*, 48. [CrossRef]
9. Matalgah, K.; Ravindranath, P.K.; Pulipati, D.; Fleck, T.J. Automated Quantification of Interlaminar Delaminations in Carbon-Fiber-Reinforced Polymers via High-Resolution Ultrasonic Testing. *Polymers* **2023**, *15*, 4691. [CrossRef]
10. Pathak, A.K.; Yokozeki, T.; Imada, M.; Kido, K. In-situ observation of tensile failure mode in cross-ply CFRP laminates using Talbot-Lau interferometry. *Compos. Struct.* **2020**, *253*, 112758. [CrossRef]
11. Mook, G.; Lange, R.; Koeser, O. Non-destructive characterisation of carbon-fibre-reinforced plastics by means of eddy-currents. *Compos. Sci. Technol.* **2001**, *61*, 865–873. [CrossRef]
12. Schulze, M.H.; Heuer, H.; Küttner, M.; Meyendorf, N. High-resolution eddy current sensor system for quality assessment of carbon fiber materials. *Microsyst. Technol.* **2010**, *16*, 791–797. [CrossRef]
13. Koyama, K.; Hoshikawa, H.; Kojima, G. Eddy current nondestructive testing for carbon fiber-reinforced composites. *J. Press. Vessel. Technol. Trans. Asme* **2013**, *135*, 041501. [CrossRef]
14. Zeng, Z.W.; Wang, T.; Sun, L.; He, R.G.; Chen, J.M. A domain decomposition finite-element method for eddy-current testing simulation. *IEEE Trans. Magn.* **2015**, *51*, 1–9. [CrossRef]
15. Zeng, Z.W.; Jiao, S.N.; Du, F.; Sun, L.; Li, J. Eddy current testing of delamination in carbon fiber reinforced polymer (CFRP): A finite element analysis. *Res. Nondestruct. Eval.* **2018**, *29*, 199–211. [CrossRef]
16. Zeng, Z.W.; Tian, Q.Z.; Wang, H.D.; Jiao, S.N.; Li, J. Testing of delamination in multidirectional carbon fiber reinforced polymer laminates using the vertical eddy current method. *Compos. Struct.* **2019**, *208*, 314–321. [CrossRef]

17. Guo, T.P.; Qiu, J.H.; Cheng, J.; Ji, H.L.; Peng, J.H. High Frequency Electromagnetic Eddy Current Testing System and Experimental Research. *Fore. Electron. Measurem. Technol.* **2015**, *34*, 4–9+13.
18. Mizukami, K.; bin Ibrahim, A.S.; Ogi, K.; Matvieieva, N.; Kharabet, I.; Schulze, M.; Heuer, H. Enhancement of sensitivity to delamination in eddy current testing of carbon fiber composites by varying probe geometry. *Compos. Struct.* **2019**, *226*, 111227. [CrossRef]
19. Machado, M.A.; Antin, K.N.; Rosado, L.S.; Vilaça, P.; Santos, T.G.; Machado, T. High-speed inspection of delamination defects in unidirectional CFRP by non-contact eddy current testing. *Compos. Part B.* **2021**, *224*, 109167. [CrossRef]
20. Xu, X.J.; Dai, T.; Luo, J.; Zhao, J.L.; Qiu, J.H.; Chen, S.L.; Chen, Z.Q. Detectability of delamination in laminated CFRPs with diverse stacking sequences using eddy current method with TR pancake coil. *NDT E Int.* **2023**, *136*, 102814. [CrossRef]
21. Ghoni, R.; Dollah, M.; Sulaiman, A.; Ibrahim, F.M. Defect characterization based on eddy current technique: Technical review. *Adv. Mech. Eng.* **2014**, *6*, 182496. [CrossRef]
22. Burke, S.K.; Ibrahim, M.E. Mutual impedance of air-cored coils above a conducting plate. *J. Phys. D Appl. Phys.* **2004**, *37*, 1857. [CrossRef]
23. Hoshikawa, H.; Koyama, K.A. new eddy current probe with minimal liftoff noise and phase information on discontinuity depth. *Mater. Eval.* **2003**, *61*, 423–427.
24. Liang, T.W.; He, Q.X.; Liang, Y.; Wang, D.H.; Chi, B. Eddy current probe parameters optimization design based on orthogonal experiment. *Appl. Mech. Mater.* **2015**, *734*, 118–124. [CrossRef]
25. Zheng, S.; Li, G.L.; Fu, Q.; Luo, K.M.; Shi, H.D.; Yang, D.; Li, Y.C. Analysis of the Factors Influencing the Trailing Infrared Characteristics of Underwater Vehicles under Surge Conditions Using the Orthogonal Method. *Appl. Sci.* **2023**, *13*, 3234. [CrossRef]
26. Cui, W.G.; Li, X.H.; Zhou, S.B.; Weng, J. Investigation on process parameters of electrospinning system through orthogonal experimental design. *J. Appl. Polym. Sci.* **2007**, *103*, 3105–3112. [CrossRef]
27. Xiao, Q.; Feng, J.; Xu, Z.; Zhang, H. Receiver signal analysis on geometry and excitation parameters of remote field eddy current probe. *IEEE Trans. Ind. Electron.* **2021**, *69*, 3088–3098. [CrossRef]
28. She, S.B.; Chen, Y.F.; He, Y.Z.; Zhou, Z.J.; Zou, X. Optimal design of remote field eddy current testing probe for ferromagnetic pipeline inspection. *Measurement* **2021**, *168*, 108306. [CrossRef]
29. Menana, H.; Féliachi, M. 3-D eddy current computation in carbon-fiber reinforced composites. *IEEE Trans. Magn.* **2009**, *45*, 1008–1011. [CrossRef]
30. Todoroki, A. Skin effect of alternating electric current on laminated CFRP. *Adv. Compos. Mater.* **2012**, *21*, 477–489. [CrossRef]
31. Lu, X.; Yi, Q.; Tian, G.Y. A comparison of feature extraction techniques for delamination of CFRP using eddy current pulse-compression thermography. *IEEE Sens. J.* **2020**, *20*, 12415–12422. [CrossRef]
32. Mizukami, K.; Hioki, S.; Moriyama, K.; Ogi, K.; Miyaji, W.; Kimura, K. Eddy-current array-probe technique for imaging near-surface and deep-lying delaminations in multidirectional carbon fiber composites. *Compos. Struct.* **2021**, *276*, 114537. [CrossRef]
33. Mizukami, K.; Mizutani, Y.; Kimura, K.; Sato, A.; Todoroki, A.; Suzuki, Y. Detection of in-plane fiber waviness in cross-ply CFRP laminates using layer selectable eddy current method. *Compos. Part A* **2016**, *82*, 108–118. [CrossRef]
34. Vaverka, F.; Smetana, M.; Gombarska, D.; Janousek, L. Diagnosis of Artificial Flaws from Eddy Current Testing Signals Based on Sweep Frequency Non-Destructive Evaluation. *Appl. Sci.* **2022**, *12*, 3732. [CrossRef]
35. Xu, X.J.; Ji, H.L.; Qiu, J.H.; Takagi, T. Detection of delamination in laminated CFRP composites using eddy current testing: Simulation and experimental study. *Int. J. Appl. Electrom.* **2018**, *57*, 177–192. [CrossRef]
36. Pasadas, D.J.; Ramos, H.G.; Baskaran, P.; Ribeiro, A.L. ECT in composite materials using double excitation coils and resonant excitation/sensing circuits. *Measurement* **2020**, *161*, 107859. [CrossRef]